IEEE Access
Multidisciplinary | Rapid Review | Open Access Journal

Received November 14, 2018, accepted November 28, 2018, date of publication December 11, 2018,
date of current version December 31, 2018.

*Digital Object Identifier 10.1109/ACCESS.2018.2885003*

# Fixed-Wing UAV Formation Control Design With Collision Avoidance Based on an Improved Artificial Potential Field

**JIALONG ZHANG, (Student Member, IEEE), JIANGUO YAN, AND PU ZHANG**
School of Automation, Northwestern Polytechnical University, Xi'an 710129, China

Corresponding author: Jialong Zhang (zjl0117@mail.nwpu.edu.cn)

This work was supported by the National Natural Science Foundation of China under Grant 60974146 and Grant 61473229.

**ABSTRACT** This paper addresses a local minima problem for multiple unmanned aerial vehicles (UAVs) in the process of collision avoidance by using the artificial potential field method, thereby enabling UAVs to avoid the obstacle effectively in 3-D space. The main contribution is to propose a collision avoidance control algorithm based on the virtual structure and the ''leader–follower'' control strategy in 3-D space that can avoid the obstacle effectively and then track the motion target. The three UAVs constitute the regular triangular formation as the control object, the virtual leader flight trajectory as the expected path, the obstacles as the simplified cylinders, and the artificial potential fields around them as approximately spherical surfaces. The attractive force of the artificial potential field can guide the virtual leader to track the target. At the same time, the follower tracks the leader to maintain the formation flight. The effect of the repulsive force can avoid the collision between the UAVs and arrange the followers such that they are evenly distributed on the spherical surface. Moreover, the follower's specific order and position are not required. The collision path of the UAV formation depends on the artificial potential field with the two composite vectors, and every UAV may choose the optimal path to avoid the obstacle and reconfigure the regular triangular formation flight after passing the obstacle. The effectiveness of the proposed collision avoidance control algorithm is fully proved by simulation tests. Meanwhile, we also provide a new concept for multi-UAV formation avoidance of an obstacle.

**INDEX TERMS** Local minima, information architecture, virtual leader, optimal path, avoidance obstacle.

## I. INTRODUCTION

With the rapid development of the computer, sensor and communication technology, a multi-UAV formation control system in the three-dimensional space has become the subject of extensive research and has a very important engineering application value, including scientific research, transportation, geological exploration, and the implementation of various safety measures to achieve the desired outcome [1]–[3].

Many formation structures, as well as different strategies and control algorithms, have been proposed by scholars in the multi-UAVs formation control system; the primary strategies include the ''leader-follower'' strategy, the behavior-based strategies, the virtual structure, and the collision avoidance of the UAV formation based on consensus control algorithm. Each of these methods has its own advantages and disadvantages. In the ''leader-follower'' method, any one UAV can be named as the leader, with the remainder of the UAVs acting as followers; the disadvantage of this control method is that there is no real-time feedback between the follower and the leader. For example, a distributed control scheme with distributed estimators was proposed by Hu and Gang [4]. The multi-UAV formation system can be realized by only knowing the distance between the leader and the followers in the noisy environment. In [5], the position of the leader and the formation of the structure are achieved without knowledge of the velocity and the dynamic model of the leader. In fact, in the ''leader-follower'' method, the virtual leader may replace the real leader; this situation represents one of the virtual structures. The followers accept the virtual leader task planning instructions to take the corresponding maneuvers. The main disadvantage of the ''leader-follower'' method is that there is no feedback information between the UAVs due to the distributed layout; thus, the probability of the collision between UAVs will increase. In the behavior-based method,

the maneuver of every UAV is controlled by its own weighted average and the desired trajectory [6]. In the virtual structure, the UAV formation system is treated as a rigid body, and every follower is controlled by the defining the dynamics of the virtual leader to make them into the predetermined virtual formation. In [7], according to the structure and dynamics model of the UAV formation, a combination of the virtual structure and the optimal path control strategy was applied to the formation architecture control, which can achieve the collision avoidance with the optimal path. The disadvantage of the virtual structure is that its implementation is the more centralized, namely, any one UAV failure will cause the whole system to fail. In [8], aiming at the measurement error of the UAV position sensor and the delay between the UAVs, a combination of the Lyapunov technique and graph theory was proposed to apply to the virtual structure; this approach can recover formation quickly after the collision avoidance. The consensus-based algorithm for the UAV cooperative formation control is a type of distributed control method that has the advantage of having network structure flexibility [9]–[14] and achieves the multi-channel integrated control obstacle avoidance. The key problem of the multi-agent system obstacle avoidance control is how to apply a consensus-based algorithm to cope with it well [15]–[17].

To effectively address the obstacle avoidance problem, this study proposes a consensus-based collision avoidance algorithm based on the improved artificial potential field. The main contributions of this study, relative to other works, are as follows:

1) In the study of the UAV collision avoidance problem, the artificial potential field method is a common application algorithm because of its advantages of being simple, practical and of high engineering practicality. A common problem with the artificial potential field method is the existence of local minima between the UAV formation system, the obstacle and the motion object; that is, when the UAV is close to the obstacle, the repulsive force is in the opposite direction of the UAV movement. At the same time, the UAV stays at the minimum and cannot reach the final target location [18]–[20]. A possible solution to this problem is to add the outside disturbance in the vertical direction or horizontal direction to break this balance. In this paper, we address a local minima problem for multiple unmanned aerial vehicles in the process of the collision avoidance by using the artificial potential field method, thereby enabling UAV avoid the obstacle effectively in three-dimensional space.

2) In this paper, the velocity of the UAV can maintain in a stable state, especially in the multi-UAV system. Gupte *et al*. [19] proposed a method of combining the artificial potential field and the electrostatic field that causes the UAV to eliminate the local minimum points in the process of the obstacle avoidance. However, this method has the limitation that the UAVs are navigated to avoid the obstacle by the artificial potential field around the stationary obstacle. In recent years, many control algorithms have been proposed by authors for the multi-UAV formation in the two-dimensional plane to follow and track the target point. In the process of the UAV collision avoidance, the control algorithm can ensure the UAV formation system maintains good stability and robustness [21]. Moreover, the UAV formation tracking motion target, the controller design is a key factor [22]. For example, the UAV can avoid the obstacle with a smooth corner and the optical path and track the motion the target to reach the target point. Moreover, some scholars proposed the UAV cooperative formation model predictive control method and studied the collision avoidance for any shape and size of obstacles that supplement and optimize the obstacle avoidance theory of the UAV formation system. The proposed collision avoidance control algorithm based on the virtual structure and the ''leader-follower'' control strategy that can avoid the obstacle effectively and then track the motion target.

3) The multi-UAV formation system predicts the motion target trajectory, avoids the obstacle, and then completes the target of tracking the movement; this is a complex process and one of the core issues to be solved. In the paper, the obstacle avoidance with the artificial potential field is easy to be trapped in local minima, an artificial potential field with an integrated vector in the three-dimensional space is proposed for application to the UAV formation. The defined leader of the UAV formation is located in the geometric center of the UAV formation structure, with the remainder of the UAVs as followers, which consist of UAVs in the regular triangle formation. The follower follows the leader and tracks the motion target until reaching the target point in the three-dimensional space. The UAV formation will approach the motion target position by the attractive force generated by the target. The attractive force causes the UAV to maintain the desired relative distance between UAVs. The motion trajectory of each UAV is the result of the resultant force of the attractive of the leader and the repulsive fields of its neighbors. The artificial potential field with the three-dimensional space vector around the obstacle is composed of two types of the potential field: the artificial potential field parallel to the $x - y$ plane and the artificial potential field parallel to the $y - z$ plane. Each type of field has two rotational vector directions: clockwise and counterclockwise. The proposed artificial potential field with an integrated vector can ensure good stability and robustness after the collision avoidance. Moreover, the rotation vector field can adjust the direction of the UAV movement if the UAV formation is close to the obstacle to avoid the local minima position. At the same time, the UAV formation system can choose the optimal path to avoid the obstacle and reconfigure the formation tracking of the motion target.

This paper is organized as follows. In Section II, we build the point mass dynamic model of UAV and introduce the classification of UAV formation flight control system, including the inner loop control system and the outer loop control system. In Section III, we build the model of UAV formation and design the collision avoidance control strategies of UAV, including the collision avoidance of every UAV and the

control strategy of the virtual leader. In Section IV, we focus on analyzing the stability of the whole process of collision avoidance for the UAV formation. In Section V, we study the collision avoidance of UAV, including the collision avoidance method of UAV and the collision avoidance path optimization of UAV based on an improved artificial potential field. In Section VI, the effectiveness of the proposed the collision avoidance control algorithm is fully proved by semi-physical simulation platform. Finally, the concluding remarks are stated in Section VII.

## II. UAV MODEL

In this paper, the regular triangle UAV formation consists of three UAVs and a virtual leader, which is taken as a control object; the three UAVs are followers in the three vertices of the regular triangle, and the virtual leader is in the triangle geometric center. The UAV dynamical equations in three-dimensional space can be described by the point mass model as follows:

$$\begin{cases} \dot{x} = V\cos\alpha_n\cos\beta_n \\ \dot{y} = V\cos\alpha_n\sin\beta_n \\ \dot{z} = V\sin\alpha_n \\ m\dot{V} = T - D - mg\sin\alpha_n \\ \dot{\alpha}_n = \dfrac{L\cos\delta_n - mg\cos\alpha_n}{mV} \\ \dot{\beta}_n = \dfrac{L\sin\delta_n}{mV\cos\alpha_n} \end{cases} \tag{1}$$

where $T$ is the engine thrust, $g$ is the gravitational acceleration, $m$ is the mass of the UAV, $D$is the damping coefficient, $L$ is the the lift force of the UAV, $\alpha_n$ is the attack angle, $\beta_n$ is the heading angle, $\delta_n$ is the banking angle, and $V$ is the air speed. The dynamics model of a UAV is shown in Fig. 1:

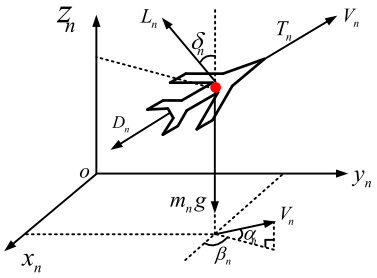


**FIGURE 1.** The UAV coordinate system model.

The UAV cooperative formation flight is divided into two types of control systems: the inner loop control system and the outer loop control system. The input signals of the inner loop control system are the engine thrust $T$, the lift force $L$ and the banking angle $\delta_n$. The output signals of outer loop will control the UAV to make the corresponding maneuver through the sensor feedback to the actuator. The nonlinear dynamics model (1) of the UAV can be pre-linearized using feedback linearization according to Eq. (2):

$$\begin{cases} \ddot{x} = \mu_x \\ \ddot{y} = \mu_y \\ \ddot{z} = \mu_z \end{cases} \tag{2}$$

where $(\mu_x, \mu_y, \mu_z)$ is the virtual acceleration, as control inputs. The virtual control input signals are defined by the linear model (2). The real control inputs are obtained by the following equation (3):

$$\begin{cases} \delta = \tan^{-1}\left(\dfrac{\mu_y\cos\beta - \mu_x\sin\beta}{(\mu_z+g)\cos\alpha - (\mu_x\cos\beta + \mu_y\sin\beta)\sin\alpha}\right) \\ L = m\dfrac{(\mu_z+g)\cos\alpha - (\mu_x\cos\beta + \mu_y\sin\beta)\sin\alpha}{\cos\delta} \\ T = m\left[(\mu_z+g)\sin\alpha + (\mu_x\cos\beta + \mu_y\sin\beta)\cos\alpha\right] + D \end{cases} \tag{3}$$

where $\tan\beta_n = \dot{y}/\dot{x}$ and $\sin\alpha_n = \dot{z}_n/V_n$.

## III. UAV FORMATION CONTROL

The regular triangle UAV formation consists of three UAVs and a virtual leader, which is taken as a control object; an improved artificial potential field algorithm is applied to the UAV formation control to achieve collision avoidance in three-dimensional space. The formation model is shown in Fig. 2:

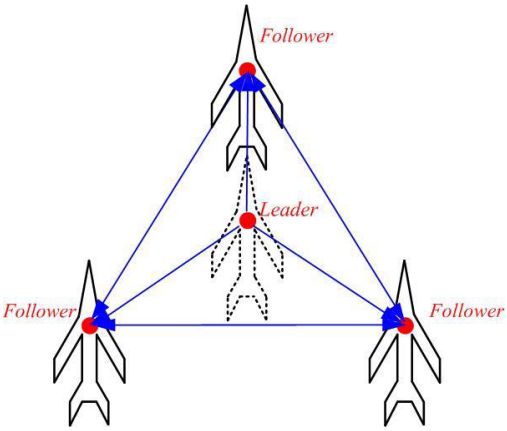


**FIGURE 2.** The UAV formation control model structure.

### A. COLLISION AVOIDANCE CONTROL ALGORITHM

The motion trajectories of every UAV in the formation are the integrated result of the control force of the two vectors. The integrated control force consists of two components, as shown in the following Eq. (4):

$$\vec{F}_n = \vec{F}_{na} + \vec{F}_r \tag{4}$$

where the first component $\vec{F}_{na}$ represents the attractive force of the artificial potential field, which can ensure that the UAV formation structure remains unchanged, and then control the

UAV to reach the spherical surface whose center is the virtual leader. $\vec{F}_{na}$ can be expressed as:

$$\vec{F}_{na} = (\vec{F}_{xna}, \vec{F}_{yna}, \vec{F}_{zna}) \tag{5}$$

where

$$\begin{cases} \vec{F}_{xna} = -k_s (x_n - x_l) \\ \left((x_n - x_l)^2 + (y_n - y_l)^2 + (z_n - z_l)^2 - r_a^2\right) \\ \vec{F}_{yna} = -k_s (y_n - y_l) \\ \left((x_n - x_l)^2 + (y_n - y_l)^2 + (z_n - z_l)^2 - r_a^2\right) \\ \vec{F}_{zna} = -k_s (z_n - z_l) \\ \left((x_n - x_l)^2 + (y_n - y_l)^2 + (z_n - z_l)^2 - r_a^2\right) \end{cases} \tag{6}$$

where $(x_l, y_l, z_l)$ represents the coordinates of the leader, and $k_s$ represents the gain coefficient. The second component $\vec{F}_r$ represents the resultant force of the repulsive force of UAV and can ensure that every UAV is evenly distributed on the spherical surface. Every UAV has a positive or negative charge, the UAVs with the same charge are repulsive to each other, and UAVs with unlike charges are attracted to each other. The control force can keep the UAVs evenly distributed on the spherical surface, whose center is $(x_l, y_l, z_l)$ and radius is $r_a$. The UAV is in a state of equilibrium if the resultant force of repulsive forces of the UAVs is tangent to the spherical surface, at the same time, the resultant force of the UAV is zero. In other words, the relative distance between any two UAVs is equal and constitutes a regular triangular formation. The three components' expression of attractive force can ensure that every UAV is evenly distributed on the spherical surface. $k_s$ represents the gain coefficient, the UAV is in a state of equilibrium by adjusting its value. Moreover, the relative distance between any two UAVs is equal and constitutes a regular triangular formation. In addition, $F_n$ is tangent to the spherical surface. The repulsive force of the UAVs is defined as follows:

$$\vec{F}_{nr} = k_r \frac{q_n q_r}{r_{nr}^2} \tag{7}$$

where $q_n$ represents the electric quantity of the $n$th UAV, $q_r$ represents the electric quantity of the $r$th UAV, $k_r$represents the repulse constant coefficient, $r_{nr}$ represents the relative distance between the $n$th UAV and the $r$th UAV. There are $N$ ($N = 3$) UAVs in the UAV formation; thus, the resultant force of the $n$th UAV from any UAV is shown in Eq. (8):

$$\vec{F}_r = k_r q_n \sum_{i=1, i\neq n}^{N} \frac{q_i}{r_{ni}^2} \tag{8}$$

The repulsive force of every UAV can be decoupled into the sub-repulsive of three coordinate axes, as shown in Fig. 3:

where $p$ is the initial position of the UAV, $P'$ denotes the position of UAV after a move, $Q_2$ is the projection of $p$ on the $X_0 - O - Y$ plane, and $Q_3$ is the projection of $P'$ on the $Z_0 - O - Q_1$ plane.

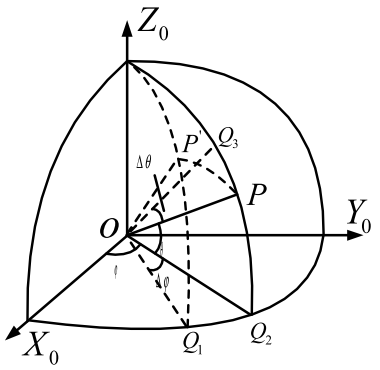


**FIGURE 3.** The UAV motion direction diagram.

$$\begin{cases} \vec{F}_{xr} = k_r q_n \sum\limits_{i=1, i\neq n}^{N} \dfrac{q_i}{r_{ni}^2} \cos\theta_{ni} \cos\varphi_{ni} \\ \vec{F}_{yr} = k_r q_n \sum\limits_{i=1, i\neq n}^{N} \dfrac{q_i}{r_{ni}^2} \cos\theta_{ni} \sin\varphi_{ni} \\ \vec{F}_{zr} = k_r q_n \sum\limits_{i=1, i\neq n}^{N} \dfrac{q_i}{r_{ni}^2} \sin\theta_{ni} \end{cases} \tag{9}$$

where

$$\begin{cases} \sin\theta_{ni} = \dfrac{z_n - z_i}{|r_{ni}|} \\ \cos\theta_{ni} = \dfrac{\sqrt{(x_n - x_i)^2 + (y_n - y_i)^2}}{|r_{ni}|} \\ \cos\varphi_{ni} = \dfrac{x_n - x_i}{\sqrt{(x_n - x_i)^2 + (y_n - y_i)^2}} \\ \sin\varphi_{ni} = \dfrac{y_n - y_i}{\sqrt{(x_n - x_i)^2 + (y_n - y_i)^2}} \\ r_{ni} = \sqrt{(x_n - x_i)^2 + (y_n - y_i)^2 + (z_n - z_i)^2} \end{cases} \tag{10}$$

and

$$\begin{cases} \vec{F}_{xn} = \vec{F}_{xna} + \vec{F}_{xr} \\ \vec{F}_{yn} = \vec{F}_{yna} + \vec{F}_{yr} \\ \vec{F}_{zn} = \vec{F}_{zna} + \vec{F}_{zr} \end{cases} \tag{11}$$

From the above Eqs. (9) and (10), we obtain that the repulsive force $F_r$ of the UAV is proportional to $1/r_{ni}$, and then the UAV can avoid an obstacle by choosing the appropriate repulsive force. In Eq. (11), the control force $\left(\vec{F}_{xn}, \vec{F}_{yn}, \vec{F}_{zn}\right)$ leads the UAV toward the spherical surface to the equilibrium position.

### B. CONTROL STRATEGY OF THE VIRTUAL LEADER

In the process of the UAV formation flight, the motion trajectory of the virtual leader as the desired path, the follower tracks the leader to constitute a regular triangle formation, and then the attractive force of the target leads the leader toward the target point. The position of the leader is $p_l = (x_l, y_l, y_l)$,

and the position of the target is $p_t = (x_l, y_l, y_l)$. The attractive force of the UAV is as follows:

*if* $r < d$

$$\begin{cases} F_{xa} = -k_t (x_l - x_t) \\ F_{ya} = -k_t (y_l - y_t) \\ F_{za} = -k_t (z_l - z_t) \end{cases} \tag{12}$$

*else*

$$\begin{cases} F_{xa} = -k_t (x_l - x_t) \dfrac{d_{lt}}{r_t} \\ F_{ya} = -k_t (y_l - y_t) \dfrac{d_{lt}}{r_t} \\ F_{za} = -k_t (z_l - z_t) \dfrac{d_{lt}}{r_t} \end{cases} \tag{13}$$

where $k_t$ is the positive constant. $d_{lt}$ indicates the relative distance of the virtual leader and the target. $d_{lt} = \sqrt{(x_l - x_t)^2 + (y_l - y_t)^2 + (z_l - z_t)^2}$, and $r_t$ indicates that the target is reduced to the radius of the sphere.

By controlling the damping force of leader, the UAV formation system can achieve the purpose of the collision avoidance if the leader is close to the target and the relative speed between them increases. The definition of damping force is shown in Eq. (14):

$$\begin{cases} F_{x_{dam}} = -k_m (\dot{x}_l - \dot{x}_t) \\ F_{y_{dam}} = -k_m (\dot{y}_l - \dot{y}_t) \\ F_{z_{dam}} = -k_m (\dot{z}_l - \dot{z}_t) \end{cases} \tag{14}$$

where $k_m$ indicates the positive coefficient; every UAV is the resultant force of the attractive force and the damp force, as shown in Eq. (15):

$$\begin{cases} F_{xl} = F_{xa} + F_{x_{dam}} \\ F_{yl} = F_{ya} + F_{y_{dam}} \\ F_{zl} = F_{za} + F_{z_{dam}} \end{cases} \tag{15}$$

Though the above analysis, the optimal control of a single UAV and the virtual leader can ensure the security of the UAV formation system collision avoidance and choose the optimal path to reach the target point.

## IV. STABILITY ANALYSIS

The UAV formation system goes through a dynamic process from the loose formation to the close formation to the collision avoidance and then to the final UAV formation; the stability of the UAV formation system is very important because it is directly related to the collision avoidance success or failure, which is of one of the key factors. This section is focused on analyzing the stability of the whole process of collision avoidance. When UAV is evenly distributed on the spherical surface, and then the UAV is in the equilibrium state with the artificial potential field; namely, the resultant force of repulsive force is zero. Hence, the effect of repulsive force is ignored. The repulsive force to the stability of the closed loop system, relative to the attractive force, is important. Firstly, the resultant force of repulsive force can make UAV formation evenly distributed on the spherical surface; secondly, it can ensure a regular triangular formation. This paper considers a regular triangular UAV formation consisting of three fixed-wing UAVs, including a leader and two followers. The UAV is in the equilibrium state if a single UAV is located on the spherical surface with the artificial potential field around the obstacle; that is, the resultant force of repulsive forces is zero. When the UAV is in motion on the spherical surface whose center is $(x_c, y_c, z_c)$ and radius is $r_a$, it is in a stable state; that is, the velocity of the UAV is zero.

***Lemma*** The desired trajectory of the UAV is satisfied by the following condition Eq. (16)

$$\begin{cases} \dot{x} = -l_r \left((x - x_c)^2 + (y - y_c)^2 + (z - z_c)^2 - r_a^2\right) \\ \dot{y} = -l_r \left((x - x_c)^2 + (y - y_c)^2 + (z - z_c)^2 - r_a^2\right) \\ \dot{z} = -l_r \left((x - x_c)^2 + (y - y_c)^2 + (z - z_c)^2 - r_a^2\right) \end{cases} \tag{16}$$

where $(x, y, z) \neq (x_c, y_c, z_c)$ and $l_r$ indicates the relative distance of the UAV and the center of the sphere.

***Proof:*** Suppose that the UAV is located on the spherical surface, so $r^2 = (x - x_c)^2 + (y - y_c)^2 + (z - z_c)^2$, and $\varphi = \arctan\left((y - y_c)/(x - x_c)\right)$. Substituting $\theta = \arctan\left((z - z_c) \Big/ \left(\sqrt{(x - x_c)^2 + (y - y_c)^2}\right)\right)$ into Eq. (6). Here, $\varphi$ and $\theta$ are shown in fig. 3. Eq. (17) is given by:

$$\dot{r} = -r\left(r^2 - r_a^2\right), \quad \dot{\theta} = 0, \ \dot{\varphi} = 0 \tag{17}$$

When the UAV is located on the spherical surface, it is obvious that $r = r_a$; similarly, $\dot{\varphi}$ and $\dot{\theta}$ converge to zero. To prove the stability of motion on the spherical surface, we define $\varepsilon = r - r_a$ and choose the Lyapunov function, as shown in Eq. (18):

$$W(\varepsilon) = \varepsilon^2 \tag{18}$$

The derivate of Eq. (18) is given by:

$$\dot{W}(\varepsilon) = 2\varepsilon r \tag{19}$$

Substituting $\varepsilon = r - r_a$ and Eq. (17) into Eq. (19), we obtain

$$\dot{W}(\varepsilon) = -2\varepsilon^2 r (r + r_a) \tag{20}$$

When $(x, y, z) \neq (x_c, y_c, z_c)$, it is obvious that for $r > 0$, we obtain $\dot{W}(\varepsilon) \leq 0$. When $r = r_a$, it is obvious that $\dot{W}(\varepsilon) = 0$. When $\dot{\theta} = 0$, $\dot{\varphi} = 0$ and $W(\varepsilon)$ is bounded, the velocity of the UAV is indirectly convergent.

## V. COLLISION AVOIDANCE STRATEGY OF UAV

In the operational mission process of the UAV formation, the collision avoidance is one of the key factors. In this paper, it is the core of the proposed avoidance algorithm that the UAV can rapidly achieve the collision avoidance with the optimal path, and then form the triangle formation. Thus, an integrated artificial potential field with rotation vector is proposed to solve this problem in the paper. In this section, the two types of control algorithms are proposed for single UAV and multi-UAV that can achieve the purpose of the collision avoidance.

### A. COLLISION AVOIDANCE METHOD OF UAV

In the process of the tracking the virtual leader, the follower's trajectory is the key to designing the collision avoidance algorithm in three-dimensional space. Suppose that the obstacle seen by the UAV visual sensor is approximately a cylinder whose surface radius is $r$ and height is $h$. In addition, suppose the artificial potential field around the cylinder is approximately ellipsoid. Suppose that the minimum volume of the artificial potential field is an ellipsoid. When the cylinder is completely covered by an ellipsoid, the artificial potential field can cover the obstacle. The geometry relationship of the artificial potential field and the obstacle is shown in Fig. 4:

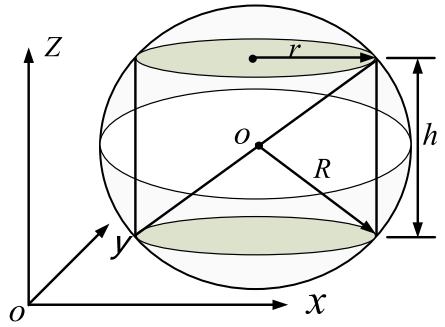


**FIGURE 4.** The geometry relationship of model.

where the ellipsoid represents the artificial potential field region, the cylinder represents the obstacle; $o$ is the center of the ellipsoid, $R$ is the radius of the ellipsoid, $r$ is the radius of the upper or lower surface of the cylinder, $h$ is height of the cylinder. Meanwhile, the artificial potential field region is minimum. The ellipsoid equation is given by

$$\frac{1}{3r^2}(x-x_0)^2+\frac{1}{3h^2}(y-y_0)^2+\frac{1}{3r^2}(z-z_0)^2=1 \quad (21)$$

The collision avoidance using the artificial potential field mainly depends on the repulsive force. When the UAV is close to the obstacle, the repulsive force of UAV is in the opposite direction of its own motion speed, and the UAV will be in the local minimum position. To avoid the local minimum position, a three-dimensional integrated artificial potential field is proposed to drive the UAV to avoid this position. The artificial potential field with a three-dimensional integrated vector covers the ellipsoid and can avoid the obstacle with the optimal path. A three-dimensional integrated artificial potential field can be composed of two types of potential fields: one is parallel to the $x-y$ plane of the potential field and the other is parallel to the $y-z$ plane of the potential field. The diagram is shown in Fig. 5:

Fig. 5 shows that the collision avoidance trajectory of UAV is the result of superposition with the two rotation potential field vectors. The UAV can rapidly avoid the obstacle with the optimal path to form the triangle formation. Here, $\theta_n$ and $\gamma_n$ are each affected by the two kinds of potential fields, as shown

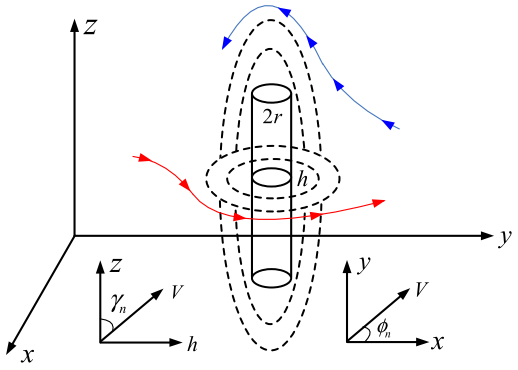


**FIGURE 5.** The rotated vector field around the obstacle in three-dimensional space.

in Eq. (22):

$$\theta_n=\arctan(\dot{y},\dot{x}),\quad \gamma_n=\arctan\left(\dot{z},\sqrt{\dot{x}^2+\dot{y}^2}\right) \quad (22)$$

The motion trajectory of UAV in the $x-y$ plane projection curve is affected by the rotation vector of the artificial potential field. The rotation vector of the artificial potential field can be divided into two directions: the clockwise and the counterclockwise directions. The kinematics model of UAV in the $x-y$ plane with rotation vector is given by Eqs. (23) and (24):

$$\begin{cases}\dot{x}=\dfrac{h}{r}(x-x_0)\\ \dot{y}=-\dfrac{r}{h}(y-y_0)\ \textit{in clockwise direction}\\ \dot{z}=0\end{cases} \quad (23)$$

$$\begin{cases}\dot{x}=-\dfrac{h}{r}(x-x_0)\\ \dot{y}=\dfrac{r}{h}(y-y_0)\ \textit{in counterclockwise direction}\\ \dot{z}=0\end{cases} \quad (24)$$

Similarly, the motion trajectory of UAV in the $y-z$ plane projection curve is affected by the rotation vector of the artificial potential field. The rotation vector of the artificial potential field can be divided into two directions, including the upward direction and the downward direction. The kinematics model of UAV in the $y-z$ plane with rotation vector is shown in Eq. (25) and (26):

$$\begin{cases}\dot{x}=\dfrac{h}{\sqrt{h^2+r^2}}(z-z_0)\cos(\phi_n)\\ \dot{y}=\dfrac{h}{\sqrt{h^2+r^2}}(z-z_0)\\ \sin(\phi_n)\ \textit{in upward direction}\\ \dot{z}=-\dfrac{\sqrt{h^2+r^2}}{h}(x-x_0)\cos(\phi_n)\\ +\dfrac{\sqrt{h^2+r^2}}{h}(y-y_0)\sin(\phi_n)\end{cases} \quad (25)$$

$$\begin{cases} \dot{x} = -\dfrac{h}{\sqrt{h^2+r^2}}(z-z_0)\cos(\phi_n) \\ \dot{y} = -\dfrac{h}{\sqrt{h^2+r^2}}(z-z_0) \\ \sin(\phi_n) \ \textit{in downward direction} \\ \dot{z} = \dfrac{\sqrt{h^2+r^2}}{h}(x-x_0)\cos(\phi_n) \\ +\dfrac{\sqrt{h^2+r^2}}{h}(y-y_0)\sin(\phi_n) \end{cases} \tag{26}$$

### B. COLLISION AVOIDANCE PATH OPTIMIZATION OF UAV

When the UAV enters the collision avoidance zone, the UAV can avoid the local minima position with the optimal path by using the collision avoidance control algorithm. In this paper, aiming at the collision avoidance of UAV, an optimization strategy is proposed. In addition, the single UAV, a multi-UAV formation system and the concept of the control force are presented in this section.

When the UAV is close to the obstacle, the artificial potential field with rotation vector causes the UAV to bypass the obstacle with the desired path. The obstacle is simplified as a sphere whose minimum radius is $r_0$, and the relative distance between the UAV and the obstacle can satisfy the following Eq. (27):

$$r_a = \sqrt{(x-x_c)^2+(y-y_c)^2+(z-z_c)^2} \tag{27}$$

The control force of UAV is given by:

$$F_{nr} = \left(F_{xnr}, F_{ynr}, F_{znr}\right) \tag{28}$$

The relationships of the control force are as follows:
*if* $r_a < r_o$

$$F_r = F_{desired} + \frac{|F_{desired}|\,F_{nr}}{r_0^2}\left(\frac{1}{r_a}-\frac{1}{r_0}\right) \tag{29}$$

*else*

$$F_r = F_{desired} \tag{30}$$

where the virtual leader control force is $F_{desired} = \left(F_{xl}, F_{yl}, F_{zl}\right)$, and every UAV control force is $F_{desired} = \left(F_{xna}+F_{nr}, F_{yna}+F_{nr}, F_{zna}+F_{nr}\right)$.

The motion trajectory of UAV is affected by the artificial potential field with rotation vector; thus, the control force for the collision avoidance is given by:

$$\begin{cases} F_{x_{rxy}} = k_0\dfrac{h}{r}(y-y_0) \\ F_{y_{rxy}} = -k_0\dfrac{h}{r}(x-x_0) \ \textit{in clockwise direction} \\ F_{z_{rxy}} = 0 \end{cases} \tag{31}$$

or

$$\begin{cases} F_{x_{rxy}} = -k_0\dfrac{h}{r}(y-y_0) \\ F_{y_{rxy}} = k_0\dfrac{h}{r}(x-x_0) \ \textit{in counterclockwise direction} \\ F_{z_{rxy}} = 0 \end{cases} \tag{32}$$

where $k_o$ is the gain coefficient. The clockwise and counterclockwise schematic diagram of the artificial field vector in the $x-y$ plane is shown in Fig. 6:

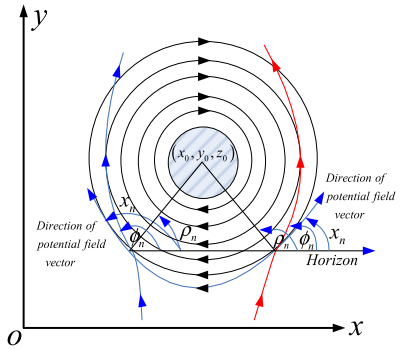


**FIGURE 6.** The clockwise and counterclockwise schematic diagram of the artificial field vector in the $x-y$ plane.

where $\rho_n$ is the angle between line linking the UVA and the center of obstacle and the positive direction of horizontal axis, $x_n$ indicates the artificial potential field vector, and $\phi_n$ is the angle between the velocity of UAV the positive direction of horizontal axis. They can be obtained as follows:

$$\begin{cases} \phi_n = \arctan(\dot{y}, \dot{x}) \\ \chi_n = \arctan\left(-r^2x_0, h^2y_0\right) \\ \rho_n = \arctan(y_0-y, x_0-x) \end{cases} \tag{33}$$

The direction of the rotation vector field around the obstacle is divided into two cases: the rotation vector field is in the clockwise direction if $\phi_n \geq \rho_n$ and the rotation vector field is in the counterclockwise direction if $\phi_n < \rho_n$.

The motion trajectory of UAV is affected by the artificial potential field with rotation vector; thus, the control force for the collision avoidance is given by:

$$\begin{cases} F_{rxyz} = k_0\dfrac{h}{\sqrt{r^2+h^2}}(z-z_0)\cos(\phi_n) \\ F_{ryyz} = k_0\dfrac{h}{\sqrt{r^2+h^2}}(z-z_0) \\ \sin(\phi_n) \ \textit{in upward direction} \\ F_{rzyz} = -k_0\dfrac{\sqrt{r^2+h^2}}{h}(x-x_0)\cos(\phi_n) \\ +\dfrac{\sqrt{r^2+h^2}}{h}(y-y_0)\sin(\phi_n) \end{cases} \tag{34}$$

or

$$\begin{cases} F_{rxyz} = -k_0\dfrac{h}{\sqrt{r^2+h^2}}(z-z_0)\cos(\phi_n) \\ F_{ryyz} = -k_0\dfrac{h}{\sqrt{r^2+h^2}}(z-z_0) \\ \sin(\phi_n) \ \textit{in downward direction} \\ F_{rzyz} = k_0\dfrac{\sqrt{r^2+h^2}}{h}(x-x_0)\cos(\phi_n) \\ -\dfrac{\sqrt{r^2+h^2}}{h}(y-y_0)\sin(\phi_n) \end{cases} \tag{35}$$

The upward and downward schematic diagram of the artificial field vector in the $y-z$ plane is shown in Fig. 7:

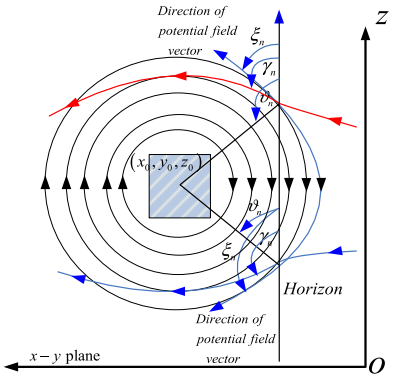


**FIGURE 7.** The upward and downward schematic diagram of the artificial field vector in the $y-z$ plane.

Where $\vartheta_n$ is the angle between the line linking the UVA and the center of obstacle and the positive direction of horizontal axis, $\zeta_n$ indicates the artificial potential field vector, and $\gamma_n$ indicates the velocity direction of the UAV. They can be obtained as follows:

$$\begin{cases} \gamma_n = \arctan\left(\dot{z}, \sqrt{\dot{x}^2+\dot{y}^2}\right) \\ \zeta_n = \arctan \\ \left[\begin{array}{c} \dfrac{h}{\sqrt{h^2+r^2}}(z-z_0), -\dfrac{\sqrt{h^2+r^2}}{h}(x-x_0)\cos(\phi) \\ -\dfrac{\sqrt{h^2+r^2}}{h}(y-y_0)\sin(\phi) \end{array}\right] \\ \vartheta_n = \arctan\left(z_0 - z, \sqrt{(x-x_0)^2+(y-y_0)^2}\right) \end{cases} \tag{36}$$

The direction of the rotation vector field around the obstacle is divided into two cases: the rotation vector field is in the upward direction if $\gamma_n \geq \vartheta_n$ and the rotation vector field is in the downward direction if $\gamma_n < \vartheta_n$. When the UAV formation system is close to the obstacle or approaches the obstacle while the UAV takes the collision avoidance action, it can be obtained the collision avoidance control force by comparing the size relationship between $|\gamma_n - \zeta_n|$ and $|\phi_n - \chi_n|$. The collision avoidance control force is as follows:

*if* $|\gamma_n - \zeta_n| < |\phi_n - \chi_n|$, then we obtain Eq. (37)

$$\begin{cases} F_{x_{nr}} = F_{x_{rxy}} \\ F_{y_{nr}} = F_{y_{rxy}} \\ F_{z_{nr}} = F_{z_{rxy}} \end{cases} \tag{37}$$

*else*

$$\begin{cases} F_{x_{nr}} = F_{x_{ryz}} \\ F_{y_{nr}} = F_{y_{ryz}} \\ F_{z_{nr}} = F_{z_{ryz}} \end{cases} \tag{38}$$

The collision avoidance control force of the UAV formation system can be normalized:

$$F_{nr} = \left(\frac{F_{x_{nr}}}{\|F_{x_{nr}}\|}, \frac{F_{y_{nr}}}{\|F_{y_{nr}}\|}, \frac{F_{z_{nr}}}{\|F_{z_{nr}}\|}\right) \tag{39}$$

## VI. SIMULATION RESULTS

The UAV formation system is composed of the four UAVs, including three UAVs and a virtual leader. The process of the transmission information is bidirectional. The obstacle is simplified as a cylinder, and the surrounding artificial is approximately ellipsoid. The UAV formation can achieve the collision avoidance by using the proposed control algorithm with a three-dimensional integrated artificial potential field. Based on the model of the UAV formation and the proposed control algorithm, we can obtain the simulation curves in different situations, as shown in Figs. 8 to 13:

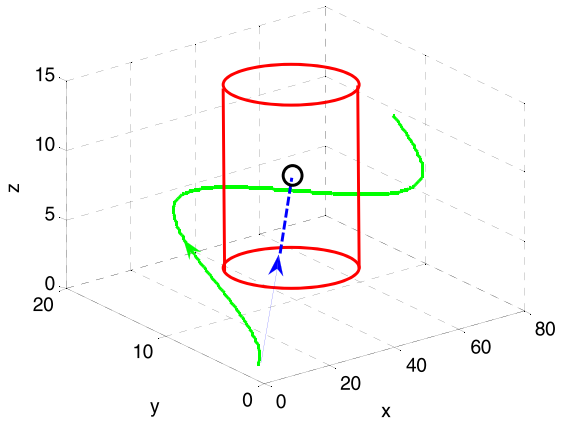


**FIGURE 8.** The collision avoidance diagram of a single UAV in the $x-y$ plane artificial potential field.

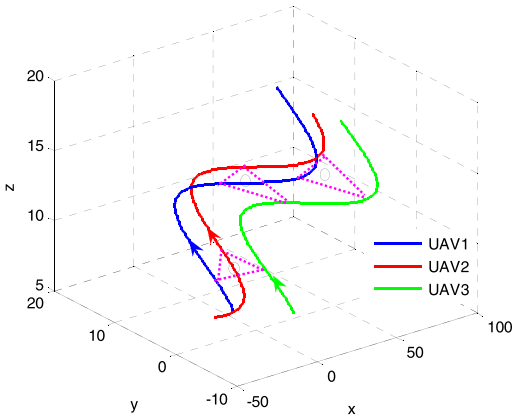


**FIGURE 9.** The whole process diagram of a UAV from loose formation to close formation.

Fig. 8 shows that the collision avoidance diagram of the UAV is parallel to the $x-y$ plane with the clockwise artificial potential field. The initial position of the UAV in the figure is (0,2,0), and the center of the obstacle is (40,10,6). Suppose that the general situation of the artificial potential field is shielded; that is, the input control force disappears while the UAV moves toward the center of the obstacle, and then it will stay in the local minimum position. At the same time, the UAV is in balance by the resultant of the repulsive force the obstacle generated and the attractive force

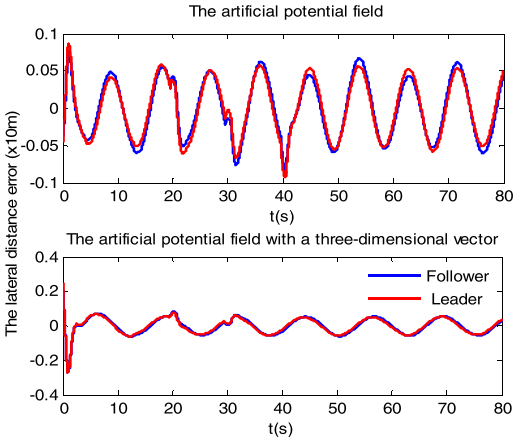


**FIGURE 10.** The comparison of the UAV lateral distance error in two types of artificial potential field.

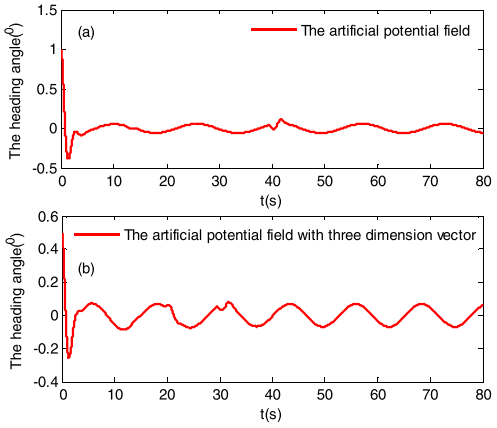


**FIGURE 11.** The comparison of the UAV heading angle variation in two types of artificial potential field.

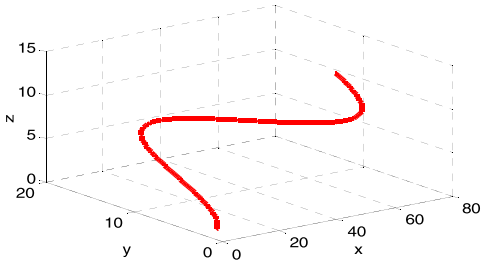


**FIGURE 12.** The UAV formation tracking motion target trajectory.

the target generated. When adding parallel to the $x-y$ plane clockwise artificial potential field, the effect of the control force can avoid the local minimum position and lead the UAV toward the obstacle movement. Similarly, the application of the parallel to the $x-y$ plane counterclockwise artificial potential field, the application of the parallel to $y-z$ the plane upward direction artificial potential field and the application of the parallel to the $y-z$ plane downward direction artificial potential field can all avoid the local minima point.

Fig. 9 shows that the UAVs are assembled into the regular triangular formation process. The initial position of the three UAVs and a virtual leader are respectively (2,2,6), (−10,2,7), (20,0,5), and (20,10,10). Based on the UAV

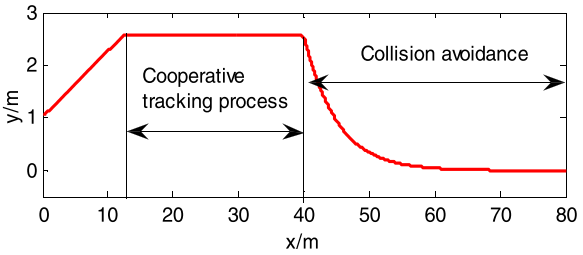


**FIGURE 13.** The relative distance of between the obstacle and the UAVs.

formation dynamics Eq. (3) and the input control force Eq. (28), the motion trajectory of the target is determined by Eq. (15), we can suppose, $F_{\mathrm{xa}} = 8$, $F_{\mathrm{ya}} = 10\cos(1/8x_v)$ and $F_{\mathrm{za}} = 2$. As seen from the figure, the UAV 2 shows the trend of slight vibration and then the automatic adjustment to quickly recover the regular triangular formation. This shows that the UAV can automatically adjust and avoid the local minimum position around the obstacle regardless of the specific order and position of the UAV in the artificial potential field.

Fig. 10 shows the comparison diagram of the UAV formation later distance error in the general artificial potential field and the artificial potential field with the rotation vector. By comparison, it is obvious that the UAV formation and the obstacle maintain a safe distance and continuously choose the optimal path of collision avoidance in the artificial potential field. The advantage of this method is that the amplitude of the lateral distance error between them is small, the dynamic response is fast and the formation is maintained.

Fig. 11 shows the comparison diagram of the change of the UAV formation heading angle. From figure 13(a), in the effect of artificial potential field, the UAV can perceive the target by the visual sensor and avoid the obstacle with the greatest safe distance. In addition, very small smooth turning with small amplitude occurs, and the vibration frequency of the curve is low, as the curve does not have a large peak or trough. The disadvantage of the collision avoidance is that the collision avoidance path is far, the fuel loss is high and the collision avoidance efficiency is low. From figure 13(b), the UAV performs continuously smooth turning and chooses the optimal path the collision avoidance in the three-dimensional artificial potential field with rotation vector; that is, the UAV is basically close to the obstacle envelope movement and the curve represents the trend of the continuous equal amplitude vibration. This shows that the trajectory of UAV is tangent to the envelope of the obstacle in the case of maintaining the safe distance, and the heading angle presents the trend of the continuous small vibration.

Figs. 12 and 13 show that the UAV formation tracking motion target trajectory and the relative distance of between the UAV formation and the obstacles, respectively. The UAV formation system goes through a dynamic process from the loose formation to the close formation to the collision avoidance and then to the final UAV formation. From 12.5m to 40m, the obstacle and the UAV have same

characteristics, the relative distance between them is constant, namely, it is 2.6m. From 40m to 80m, the relative distance between them decreases slowly because the UAVs avoid the motion target during this process.

## VII. CONCLUSIONS

In the paper, an integrated artificial potential field in three-dimensional space based on the virtual structure and a ''leader-follower'' control strategy was proposed to solve the problem that the UAV formation system becomes trapped in a local minimum position in the process of collision avoidance. A integrated artificial potential field is the resultant field of the two types of field with a rotation vector, including the potential field that is parallel to the $x - y$ plane and the potential field that is parallel to the $y - z$ plane, that can make the UAV avoid each local minimum position around the obstacle and bypass the obstacle with the rapid speed and the optimal path. The UAV assembles the formation flight after the collision avoidance. In the whole process of collision avoidance, the artificial potential field force leads the three UAVs and the virtual leader to maintain the regular triangular formation while driving the UAV formation toward the target point. The repulsive force of the artificial potential field can achieve the collision avoidance between the UAVs while avoiding the collision between the UAV and the obstacle and then achieve the purpose of avoiding the obstacle.

However, a collision between the UAVs may occur if the artificial potential field around the obstacle generated is weak or the speed of the UAV is too high, making this control algorithm ineffective and possibly even destructive. Therefore, a variety of factors should be considered when implementing the algorithm in engineering practice.

## REFERENCES

[1] E. J. Forsmo, E. I. Grøtli, T. I. Fossen, and T. A. Johansen, ''Optimal search mission with unmanned aerial vehicles using mixed integer linear programming,'' in *Proc. Int. Conf. Unmanned Aircr. Syst. (ICUAS)*, May 2013, pp. 253–259.

[2] X. Kong *et al.*, ''Mobility dataset generation for vehicular social networks based on floating car data,'' *IEEE Trans. Veh. Technol.*, vol. 67, no. 5, pp. 3874–3886, May 2018, doi: 10.1109/TVT.2017.2788441.

[3] X. Kong, X. Song, F. Xia, H. Guo, J. Wang, and A. Tolba, ''LoTAD: Long-term traffic anomaly detection based on crowdsourced bus trajectory data,'' *World Wide Web*, vol. 21, pp. 825–847, May 2018, doi: 10.1007/s11280-017-0487-4.

[4] J. Hu and F. Gang, ''Distributed tracking control of leader–follower multi-agent systems under noisy measurement,'' *Automatica*, vol. 46, no. 8, pp. 1382–1387, 2010.

[5] R. Cui, S. S. Ge, B. V. E. How, and Y. S. Choo, ''Leader–follower formation control of underactuated autonomous underwater vehicles,'' *Ocean Eng.*, vol. 37, nos. 17–18, pp. 1491–1502, 2010.

[6] S. Monteiro and E. Bicho, ''A dynamical systems approach to behavior-based formation control,'' in *Proc. IEEE Int. Conf. Robot. Automat. (ICRA)*, May 2002, pp. 2606–2611.

[7] J. Ghommam, M. Saad, and F. Mnif, ''Formation path following control of unicycle-type mobile robots,'' in *Proc. IEEE Int. Conf. Robot. Automat.*, May 2010, pp. 1966–1972.

[8] H. Mehrjerdi, J. Ghommam, and M. Saad, ''Nonlinear coordination control for a group of mobile robots using a virtual structure,'' *Mechatronics*, vol. 21, no. 7, pp. 1147–1155, 2011.

[9] Q. Min *et al.*, ''Research on UAV cooperative formation flight based on 3D program control,'' *Meas. Control Technol.*, 2017.

[10] Y. Li, G. Zhou, W. Chen, and S. Zhang, *Design of UAV Close Formation Controller Based on Sliding Mode Variable Structure*. 2017.

[11] W. Ren, ''Consensus tracking under directed interaction topologies: Algorithms and experiments,'' *IEEE Trans. Control Syst. Technol.*, vol. 18, no. 1, pp. 230–237, Jan. 2010.

[12] Y. Wang, D. Wang, and J. Wang, ''A convex optimization based method for multiple UAV autonomous formation reconfiguration,'' *Scientia Sinica*, vol. 47, no. 3, pp. 249–258, 2017.

[13] J.-C. Trujillo, R. Munguia, E. Guerra, and A. Grau, ''Cooperative monocular-based SLAM for multi-UAV systems in GPS-denied environments,'' *Sensors*, vol. 18, no. 5, p. 1351, 2018.

[14] S. Cao *et al.*, ''UWB based integrated communication and positioning system for multi-UAVs close formation,'' in *Proc. Int. Conf. Mech., Electron., Control Automat. Eng.*. 2018.

[15] C. Yoshioka and T. Namerikawa, ''Observer-based consensus control strategy for multi-agent system with communication time delay,'' in *Proc. IEEE Int. Conf. Control Appl.*, Sep. 2008, pp. 1037–1042.

[16] H. Kawakami and T. Namerikawa, ''Cooperative target-capturing strategy for multi-vehicle systems with dynamic network topology,'' in *Proc. Amer. Control Conf.*, Jun. 2009, pp. 635–640.

[17] Y. Kuriki and T. Namerikawa, ''Formation control of UAVs with a fourth-order flight dynamics,'' in *Proc. IEEE Conf. Decis. Control*, Dec. 2014, pp. 6706–6711.

[18] F. Flacco, T. Kröger, A. De Luca, and O. Khatib, ''A depth space approach to human-robot collision avoidance,'' in *Proc. IEEE Int. Conf. Robot. Automat.*, May 2012, pp. 338–345.

[19] S. Gupte, O. Masoud, R. F. K. Martin, and N. P. Papanikolopoulos, ''Detection and classification of vehicles,'' *IEEE Trans. Intell. Transp. Syst.*, vol. 3, no. 1, pp. 37–47, Mar. 2002.

[20] A. Widyotriatmo and K.-S. Hong, ''Navigation function-based control of multiple wheeled vehicles,'' *IEEE Trans. Ind. Electron.*, vol. 58, no. 5, pp. 1896–1906, May 2011.

[21] K. Chang, Y. Xia, and K. Huang, ''Coordinated formation control design with obstacle avoidance in three-dimensional space,'' *J. Franklin Inst.*, vol. 352, no. 12, pp. 5779–5795, 2015.

[22] X. Dong, Y. Zhou, Z. Ren, and Y. Zhong, ''Time-varying formation tracking for second-order multi-agent systems subjected to switching topologies with application to quadrotor formation flying,'' *IEEE Trans. Ind. Electron.*, vol. 64, no. 6, pp. 5014–5024, Jun. 2017.

**JIALONG ZHANG** received the B.Eng. degree from the North China Institute of Aerospace Engineering, in 2014, and the M.E. degree from the College of Aeronautics and Astronautics Engineering, Air Force Engineering University, in 2017. He is currently pursuing the Ph.D. degree with the School of Automation, Northwestern Polytechnical University. His main research interest includes cooperative unmanned aerial vehicle formation flight control.

**JIANGUO YAN** received the B.Eng. degree from the College of Astronautics Engineering, National University of Defense Technology, in 1983, and the Ph.D. degree from the School of Automation Control, Northwestern Polytechnical University, in 2007. His research interests include computer control and intelligent control, pattern recognition, robust control, navigation, guidance and flight control, and optical flight control.

**PU ZHANG** received the B.Eng. and M.Eng. degrees from the North China Institute of Aerospace Engineering, in 2008 and 2012, respectively. She is currently pursuing the Ph.D. degree with Northwestern Polytechnical University. Her main research interests include management and optimization.